A Predictive Model for Human-Unmanned Vehicle Systems

Jacob W. Crandall *
Masdar Institute of Science and Technology, Abu Dhabi, UAE

M. L. Cummings,†
Massachusetts Institute of Technology, Cambridge MA 02139

Carl E. Nehme ‡
McKinsey & Company, Dubai, UAE

Advances in automation are making it possible for a single operator to control multiple unmanned vehicles (UVs). However, the complex nature of these teams presents a difficult and exciting challenge for designers of human-UV systems. To build such systems effectively, models must be developed that *describe* the behavior of the human-UV team and that *predict* how alterations in team composition and system design will affect the system's overall performance. In this paper, we present a method for modeling human-UV systems consisting of a single operator and multiple independent UVs. Via a case study, we demonstrate that the resulting models provide an accurate description of observed human-UV systems. Additionally, we demonstrate that the models can be used to predict how changes in the human-UV interface and the UVs' autonomy alter the system's performance.

I. Introduction

Many important missions, including search and rescue, border security, and military operations, require human reasoning to be combined with automated unmanned vehicle (UV) capabilities to form a synergistic human-UV system. However, the design and implementation of such systems remains a difficult and challenging task. Challenges related to the operators, the UVs, and the interactions between them must be addressed before human-UV systems will realize their full potentials.

To understand and address these issues more fully, comprehensive models of human-UV systems should be developed. These models should have two important capabilities. First, they should adequately *describe* the behavior and performance of the team and the system as a whole. Second, these models should be able to accurately *predict* the behavior and performance of the team as the environment, mission, or human-UV system changes.

Models with both descriptive and predictive abilities have a number of important uses. For example, such models can improve the design processes of human-UV systems. As in any systems engineering process, test and evaluation plays a critical role in fielding new technologies. In systems with significant human-automation interaction, testing with representative users is expensive and time consuming. Thus, the development of a high-fidelity model of a human-UV system with both descriptive and predictive capabilities could streamline the test and evaluation cycle by diagnosing causes of previous system failures and inefficiencies, and indicating how potential design modifications will affect the behavior and performance of the system.

A model with both descriptive and predictive capabilities can also be used to determine successful team compositions. The composition of human-UV teams can potentially change dynamically both in number and

*Assistant Professor, Information Technology Program, Abu Dhabi, UAE
†Associate Professor, Department of Aeronautics and Astronautics, Cambridge MA 02139. AIAA Associate Fellow
‡Associate, McKinsey & Company, Dubai, UAE

type of UVs due to changing mission assignments and resource availability. High-fidelity models can be used to ensure that changes in team composition will not cause system performance to drop below acceptable levels. Furthermore, given the team composition, these models can suggest which autonomy levels the UVs should employ.

As a step toward developing such high-fidelity and comprehensive models, we propose a method for modeling human-UV systems. Due to the need to reduce manning in current human-UV systems,[1] we focus on modeling human-UV systems consisting of a single operator and multiple homogeneous and independent UVs. The modeling method can be used to model systems employing any level of automation.[2–5] However, we assume that the operator interacts with each UV in the team individually, rather than in a group.[6]

The remainder of this paper proceeds as follows. In Section II, we define a stochastic model of human-UV systems consisting of a single operator and multiple independent UVs. Section III describes how this stochastic model is constructed using observational data. In Section IV, we describe a user study in which users controlled simulated UVs to perform a search and rescue mission. Observational data from this study is used to model the human-UV team and predict how changes in the system would alter its performance. In Section V, these predictions are compared with observed results. We conclude and discuss future work in Section VI.

II. Modeling Human-UV Systems

The behavior of a human-UV system consisting of a single operator and multiple independent UVs can be described with a set of models.[7] Each model describes the behavior of a particular aspect of the supervisory control system given a characterization of the system's state. In this paper, we use separate models to describe the behaviors of the operator and the individual UVs in the system. When combined, these individual models form a description of the behavior of the entire human-UV system. In this section, we describe the separate models and how they are combined. We begin by defining useful notation and terminology.

II.A. Notation and Terminology

The models described in this paper are characterized by the notion of *system state*, which we define with the tuple $\boldsymbol{\sigma} = (\boldsymbol{s}, \tau)$. The first element, $\boldsymbol{s}$, characterizes the state of each of the individual UVs in the team. Let S be the set of possible UV states, and let $s_i \in S$ be the *state* of UV i. Then, $\boldsymbol{s} = (s_1, \cdots, s_N)$ is the *joint state* of a team of N UVs. The second element of system state $\boldsymbol{\sigma}$ is *mission time* τ. Mission time, which is important to consider when modeling time-critical operations, refers to the time elapsed since the team began performing its current mission. We denote $\boldsymbol{\Sigma}$ as the set of possible system states.

II.B. Modeling UV Behavior

In previous work, the performance of a UV is modeled with respect to the temporal metrics of *neglect time* and *interaction time*.[8–10] Neglect time is the expected amount of time that a UV maintains acceptable performance levels in the absence of *interactions* (with the operator). Interaction time is the average amount of time an operator must interact with a UV to restore or maintain desirable UV performance levels. Paired together, these metrics identify the automated capability of a UV as well as the average frequency and duration of interactions necessary to keep the UV's performance above some threshold.[10] In particular, neglect time and interaction time can be used to estimate the amount of time an operator must devote to a single UV[11] and the maximum number of UVs that a single operator can effectively control (Fan-out).[9]

While neglect time and interaction time are valuable and informative metrics, they are not rich enough to sufficiently describe and predict many relevant aspects of UV behavior.[7] One potential alternative is to model UV behavior with two sets of random processes,[7,10] which we call *interaction impact* ($\mathcal{II}$) and *neglect impact* ($\mathcal{NI}$), respectively. These random processes describe a UV's behavior or performance in the presence and absence of interactions, respectively.

In this paper, we model UV behavior with state transitions. Thus, the random processes $\mathcal{II}$ and $\mathcal{NI}$ describe how a UV's state changes over time. Formally, let $\boldsymbol{\sigma} \in \boldsymbol{\Sigma}$ be the system state when the operator begins interacting with UV i. The random process $\mathcal{II}(\boldsymbol{\sigma})$ stochastically models how UV i's behavior changes its state s_i throughout the duration of the interaction. The time variable of the process takes on all values in the interval $[0, L]$, where L is the length of the interaction and $t = 0$ corresponds to the time that

the interaction began. Thus, for each $t \in [0, L]$, $\mathcal{II}(\boldsymbol{\sigma}; t)$ is a random variable that specifies a probability distribution over UV states.

Likewise, we model the behavior of a UV in the absence of human attention with a random process. Let $\boldsymbol{\sigma} \in \boldsymbol{\Sigma}$ be the system's state at the end of the UV's last interaction. Then, the random process $\mathcal{NI}(\boldsymbol{\sigma})$ describes the UV's state transitions over time in the absence of additional interactions. Hence, for each $t \in [0, \infty)$, where $t = 0$ corresponds to the time that the UV's last interaction ended, $\mathcal{NI}(\boldsymbol{\sigma}; t)$ is a random variable that specifies a probability distribution over UV states.

We note that the structures $\mathcal{II}(\boldsymbol{\sigma})$ and $\mathcal{NI}(\boldsymbol{\sigma})$ assume that UV behavior is Markovian with respect to the system state $\boldsymbol{\sigma}$ at the beginning and end of the interaction, respectively. In large part, the accuracy of the Markov assumption is dependent on the set of UV states (S). We note also that when the UVs perform independent tasks, the behavior of each individual UV in the presence and absence of interactions is independent of the states of the other UVs in the team. Since we assume independence in this paper, $\mathcal{II}(\boldsymbol{\sigma}) = \mathcal{II}(s_i, \tau)$ and $\mathcal{NI}(\boldsymbol{\sigma}) = \mathcal{NI}(s_i, \tau)$.

II.C. Modeling Operator Behavior

The operator plays a crucial role in the success of a human-UV system. Thus, a high-fidelity model of a human-UV system must account for the behavior of the operator. Since $\mathcal{II}(\boldsymbol{\sigma})$ and $\mathcal{NI}(\boldsymbol{\sigma})$ are driven by human input, they implicitly model human behavior during interactions. However, these structures do not account for how the operator allocates attention to the various UVs in the team. Previous work has identified two important aspects of operator attention allocation: *selection strategy* and *switching time*. The operator's selection strategy refers to how the operator prioritizes multiple tasks.[12–14] Switching time is the amount of time the operator spends determining which UV to service.[15,16]

As with UV behavior, temporal metrics can be used to measure operator attention allocation. One such set of metrics involves the concept of *wait times*, or times that UVs spend in degraded performance states.[13,17,18] High wait times typically indicate less effective prioritization schemes and longer switching times. Such metrics have been used to augment Fan-out predictions.[17,18]

However, as with UV behavior, we model operator switching times ($\mathcal{ST}$) and selection strategies ($\mathcal{SS}$) stochastically. Let $\mathcal{ST}(\boldsymbol{\sigma})$, where $\boldsymbol{\sigma}$ is the system state at the end of the previous interaction, be a random variable describing the length of time the operator spends selecting a UV to service. $\mathcal{ST}(\boldsymbol{\sigma})$ is a combination of two kinds of time periods. First, it consists of the time it takes for the operator to orient to the circumstances of the UVs in the team and select a UV to service. Second, it consists of time periods in which the operator monitors the UVs' progress rather than servicing any particular UV. While it is often desirable to distinguish between these two time periods, doing so requires knowledge of operator intentions, which we leave to future work.

Similarly, let $\mathcal{SS}(\boldsymbol{\sigma})$ be a random variable modeling the operator's selection strategy given the system state $\boldsymbol{\sigma}$. This random variable specifies how likely the operator selects each UV in the team. More specifically, since a UV is characterized by its state, $\mathcal{SS}(\boldsymbol{\sigma})$ is a probability distribution over UV states.

We note that operator behavior in human-UV systems is driven by a number of important cognitive processes and limitations. These processes and limitations include, among others, operator workload,[19] operator utilization,[20–22] operator trust in automation,[23,26] and operator situation awareness.[24,25] Accurate models of $\mathcal{ST}(\boldsymbol{\sigma})$, $\mathcal{SS}(\boldsymbol{\sigma})$, and to some extent $\mathcal{II}(\boldsymbol{\sigma})$, implicitly account for these cognitive phenomena.

II.D. Comprehensive Model

Since the structures $\mathcal{II}(\boldsymbol{\sigma})$, $\mathcal{NI}(\boldsymbol{\sigma})$, $\mathcal{ST}(\boldsymbol{\sigma})$, and $\mathcal{SS}(\boldsymbol{\sigma})$ are each characterized by system state $\boldsymbol{\sigma}$, they can be combined via a discrete event simulation to estimate the behavior of the human-UV system as a whole. Thus, given accurate estimates of these four structures, a high-fidelity description of the human-UV system can be constructed.

III. Modeling Human-UV Teams with Observational Data

Once a human-UV system is implemented and deployed, observational data can be used to estimate $\mathcal{II}(\boldsymbol{\sigma})$, $\mathcal{NI}(\boldsymbol{\sigma})$, $\mathcal{ST}(\boldsymbol{\sigma})$, and $\mathcal{SS}(\boldsymbol{\sigma})$ for all $\boldsymbol{\sigma} \in \Sigma$. We describe how such estimates can be formed in this section. We also formalize the discrete event simulation used to simulate the behavior of the complete human-UV system using these model estimates.

Table 1. Hypothetical observational data for a three-UV team for the mission times $\tau \in [0, 17]$. For each discrete time period τ, the system records the UV that the operate was servicing as well as the state of each UV.

Time (τ)	**0**	**1**	**2**	**3**	**4**	**5**	**6**	**7**	**8**	**9**	**10**	**11**	**12**	**13**	**14**	**15**	**16**	**17**
Operator	1	1	1			3	3			1	1	1	1			2	2	
UV 1	s^1	s^2	s^2	s^2	s^2	s^2	s^3	s^3	s^3	s^3	s^4	s^4	s^2	s^2	s^2	s^3	s^4	s^4
UV 2	s^1	s^1	s^1	s^1	s^1	s^1	s^1	s^1	s^1	s^1	s^1	s^1	s^1	s^1	s^1	s^1	s^3	s^3
UV 3	s^1	s^1	s^1	s^1	s^1	s^1	s^2	s^2	s^2	s^3	s^3	s^3	s^3	s^4	s^4	s^3	s^3	s^4

Table 2. The set of samples of interaction impact ($\Theta^{\mathcal{II}}$) derived from the hypothetical data log shown in Table 1.

UV	**System State ($x^{\boldsymbol{\sigma}}$)**		**Outcome (x^o): Sequence of States**
	x^{s_i}	x^τ	
1	s^1	0	s^1, s^2, s^2
3	s^1	5	s^1, s^2
1	s^3	9	s^3, s^4, s^4, s^2
2	s^1	15	s^1, s^3

III.A. Constructing the Individual Behavioral Models

Observational data required to model $\mathcal{II}(\boldsymbol{\sigma})$, $\mathcal{NI}(\boldsymbol{\sigma})$, $\mathcal{ST}(\boldsymbol{\sigma})$, and $\mathcal{SS}(\boldsymbol{\sigma})$ is exemplified in Table 1, which shows the data log of a hypothetical three-robot team during mission times $\tau \in [0, 17]$. At discrete time steps of unit length, the system records the UV that the operator was servicing during that time (row labeled "Operator"), and the current state of each UV in the team (rows labeled "UV 1", "UV 2", and "UV 3", respectively). For example, at time period $\tau = 2$, the table shows that the operator was servicing UV 1, UV 1 was in state s^2, and UVs 2 and 3 were both in state s^1.

From this data, samples of interaction impact, neglect impact, operator switching time, and operator selection strategies are extracted. Probability distributions over these various data samples are then derived to approximate $\mathcal{II}(\boldsymbol{\sigma})$, $\mathcal{NI}(\boldsymbol{\sigma})$, $\mathcal{ST}(\boldsymbol{\sigma})$, and $\mathcal{SS}(\boldsymbol{\sigma})$ for each $\boldsymbol{\sigma} \in \boldsymbol{\Sigma}$.

III.A.1. Extracting Data Samples

Regardless of its type (II, NI, ST, and SS), each sample $\boldsymbol{x}$ extracted from observational data is a tuple $\boldsymbol{x} = (\boldsymbol{x}^{\boldsymbol{\sigma}}, x^o)$, where $\boldsymbol{x}^{\boldsymbol{\sigma}}$ is the system state of the sample, and x^o is the outcome. Since the outcome x^o of the sample has a different form for each sample type, we discuss each sample type separately.

Samples of type II. Let $\Theta^{\mathcal{II}}$ denote the set of samples of interaction impact extracted from the observational data. For each sample $\boldsymbol{x} \in \Theta^{\mathcal{II}}$, $\boldsymbol{x}^{\boldsymbol{\sigma}} = (x^{s_i}, x^\tau)$ is the system state (assuming UVs perform independent tasks) at the beginning of an interaction with UV i. The outcome x^o of each of these samples is the sequence of states visited by the UV during the interaction. For example, Table 2 shows the four samples of interaction impact, one for each interaction, in the hypothetical data log of Table 1. The first entry of Table 2 shows the sample corresponding to the operator's interactions with UV 1 during time $\tau \in [0, 2]$. Thus, the sample's system state consists of the state of UV 1 (s^1), and the mission time $\tau = 0$. The outcome of the sample is the sequence of states that UV 1 visited during the duration of the interaction. Thus, x^o is the sequence (s^1, s^2, s^2).

Samples of type NI. Corresponding to each sample in the set $\Theta^{\mathcal{II}}$ is a sample of neglect impact, or a sample of the UV's behavior in the absence of interactions. Let $\Theta^{\mathcal{NI}}$ denote the set of samples of neglect impact extracted from the observational data. The system state $\boldsymbol{x}^{\boldsymbol{\sigma}} = (x^{s_i}, x^\tau)$ for each sample $\boldsymbol{x} \in \Theta^{\mathcal{NI}}$ is the system's state at the end of the UV's last interaction. The outcome x^o for these samples is the sequence of states the UV visits thereafter in the absence of interactions.

Table 3 shows the four samples of neglect impact extracted from the hypothetical data log in Table 1. The first entry of Table 3 shows UV 1's behavior after it is neglected by the operator at time $\tau = 3$. At this time, $x^{s_i} = s^2$, and the sequence of states visited by UV 1 thereafter (for $\tau \in [3, 9]$) was $x^o = (s^2, s^2, s^2, s^3, s^3, s^3)$.

Table 3. The set of samples of neglect impact ($\Theta^{\mathcal{NI}}$) derived from the hypothetical data log shown in Table 1.

UV	System State ($\boldsymbol{x^{\sigma}}$)		Outcome (x^o): Sequence of States
	x^{s_i}	x^{τ}	
1	s^2	3	s^2, s^2, s^2, s^3, s^3, s^3
3	s^2	7	s^2, s^2, s^3, s^3, s^3, s^3, s^4, s^4, s^3, s^3, s^4, $\cdots$
1	s^2	13	s^2, s^2, s^3, s^4, s^4, $\cdots$
2	s^3	17	s^3, $\cdots$

Table 4. The set of samples $\Theta^{\mathcal{ST}}$ of operator switching time's extracted from the hypothetical data in Table 1.

System State ($\boldsymbol{x^{\sigma}}$)		Outcome (x^o): Switching Time
$\boldsymbol{x^s}$	x^{τ}	
(s^2, s^1, s^1)	3	2
(s^3, s^1, s^2)	7	2
(s^2, s^1, s^4)	13	3
(s^4, s^3, s^4)	17	Not available

At time $\tau = 9$, however, the sequence ends in the data due to the operator again interacting with UV 1. Since a sequence of neglect impact is theoretically infinite, it may sometimes be necessary to approximate the missing portion of the sequence.

This can be done in two ways. First, knowledge of the UV's position and trajectory in the world as well as its behavioral logic, could be used to estimate the missing portion of the sequence via simulation. Second, existing samples in $\Theta^{\mathcal{NI}}$ for which the UV visited similar states can be used to approximate what the UV's state would have been in the absence of interactions. For example, the ending subsequence of the first sample (*i.e.*, s^2, s^3, s^3, s^3) is present in the outcome of the second sample. Thus, the subsequent sequence of UV states shown in the second sample's outcome (i.e., s^3, s^4, s^4, s^3, s^3, s^4, $\cdots$) could be used to approximate the missing portion of the first sample.

Samples of type ST. After each logged interaction is a sample of operator switching time. Let $\Theta^{\mathcal{ST}}$ be the set of switching time samples. The system state $\boldsymbol{x^{\sigma}} = (\boldsymbol{x^s}, x^{\tau})$ of each sample $\boldsymbol{x} \in \Theta^{\mathcal{ST}}$ is the system's state at the end of the last interaction. The outcome x^o is the time elapsed between the end of the previous interaction and the beginning of the new interaction. Table 4 shows $\Theta^{\mathcal{ST}}$ for the hypothetical data log (Table 1). For example, the first entry in the table shows that after interacting with UV 1 during time $\tau \in [0, 2]$, the operator took two time units to select UV 3. Thus, $x^o = 2$ for this sample.

Samples of type SS. Each time the operator selects a UV to service, we obtain a sample of the operator's selection strategy. The system state $\boldsymbol{x^{\sigma}} = (\boldsymbol{x^s}, x^{\tau})$ of these samples, which are gathered in the set $\Theta^{\mathcal{SS}}$, is the system state at the time the operator begins servicing the UV. The outcome x^o of the samples is the state of the UV the operator services. Table 5 shows the set of samples of the operator's selection strategy extracted from the hypothetical data log (Table 1).

III.A.2. Approximating the Stochastic Models from Data Samples

The structures $\mathcal{II}(\boldsymbol{\sigma})$, $\mathcal{NI}(\boldsymbol{\sigma})$, $\mathcal{ST}(\boldsymbol{\sigma})$, and $\mathcal{SS}(\boldsymbol{\sigma})$ can be approximated for all $\boldsymbol{\sigma} \in \boldsymbol{\Sigma}$ by forming probability distributions over the outcomes x^o of the samples in the sets $\Theta^{\mathcal{II}}$, $\Theta^{\mathcal{NI}}$, $\Theta^{\mathcal{ST}}$, and $\Theta^{\mathcal{SS}}$, respectively. These probability distributions are based on the distance between each sample's system state $\boldsymbol{x^{\sigma}}$ and the target system state $\boldsymbol{\sigma}$. Formally, the probability that the outcome x^o from some sample $\boldsymbol{x} \in \Theta$ defines the behavior of a UV or the operator (as the case may be) is:

$$Pr(x^o|\boldsymbol{\sigma}, \Theta) = \frac{w^T(\boldsymbol{x}|\boldsymbol{\sigma})}{\sum_{\boldsymbol{y}\in\Theta} w^T(\boldsymbol{y}|\boldsymbol{\sigma})}, \tag{1}$$

Table 5. The set of samples $\Theta^{\mathcal{SS}}$ for operator selection strategies extracted from the hypothetical data in Table 1.

System State ($\boldsymbol{x^\sigma}$)		Outcome (x^o): State of Selected UV
$\boldsymbol{x^s}$	x^τ	
(s^1, s^1, s^1)	0	s^1
(s^2, s^1, s^1)	5	s^1
(s^3, s^1, s^3)	9	s^3
(s^3, s^1, s^3)	15	s^1

where $w^T(\boldsymbol{x}|\boldsymbol{\sigma})$ is the weight of sample $\boldsymbol{x}$ given the system state $\boldsymbol{\sigma}$ and the type $T \in \{II, NI, ST, SS\}$ of samples in Θ.

The weight $w^T(\boldsymbol{x}|\boldsymbol{\sigma})$ is computed differently depending on the sample type T. To compute probability distributions to estimate $\mathcal{II}(\boldsymbol{\sigma})$ and $\mathcal{NI}(\boldsymbol{\sigma})$, the weights $w^{II}(\boldsymbol{x}|\boldsymbol{\sigma})$ and $w^{NI}(\boldsymbol{x}|\boldsymbol{\sigma})$ are:

$$w^{II}(\boldsymbol{x}|\boldsymbol{\sigma}) = w^{NI}(\boldsymbol{x}|\boldsymbol{\sigma}) = f(x^\tau - \tau) \cdot \boldsymbol{I}_{s_i}(x^{s_i}). \tag{2}$$

The function $f(x^\tau - \tau)$ produces values in the range $[0, 1]$, and returns higher values when $x^\tau - \tau$ is small. The indicator function $\boldsymbol{I}_{s_i}(x^{s_i})$ returns unity if $s_i = x^{s_i}$, and zero otherwise. Thus, in words, the weight of sample $\boldsymbol{x} \in \Theta^{\mathcal{II}}$ is zero if the target UV state s_i is equal to the sample's UV state x^{s_i}. Otherwise, the weight of $\boldsymbol{x}$ is a function of the proximity of the target mission time τ to the sample's mission time x^τ.

Calculating $w^{ST}(\boldsymbol{x}|\boldsymbol{\sigma})$ is slightly more involved than calculating $w^{II}(\boldsymbol{x}|\boldsymbol{\sigma})$ and $w^{NI}(\boldsymbol{x}|\boldsymbol{\sigma})$, since the system state $\boldsymbol{x^\sigma}$ of each sample $\boldsymbol{x} \in \Theta^{\mathcal{ST}}$ includes the joint state $\boldsymbol{x^s}$ rather then just x^{s_i}. Thus, to determine, $w^{ST}(\boldsymbol{x}|\boldsymbol{\sigma})$, the similarity between $\boldsymbol{s}$ and $\boldsymbol{x^s}$ must also be determined. Let $\boldsymbol{V^x}$ be the set of permutation vectors of $\boldsymbol{x^s}$ and let v^{x_i} be the i^{th} element of the vector $\mathbf{v^x} \in \boldsymbol{V^x}$. Then, the similarity between the joint states $\boldsymbol{s}$ and $\boldsymbol{x^s}$ is given by

$$\Phi(\boldsymbol{s}, \boldsymbol{x^s}) = \min_{\boldsymbol{v^x} \in \boldsymbol{V^x}} \prod_{i=1}^{n} \phi(s_i, v^{x_i}), \tag{3}$$

where $\phi(s_i, v^{x_i}) \in [0, 1]$ is the similarity between the individual UV states s_i and v^{x_i}, and $\phi(s_i, v^{x_i}) = 1$ when $s_i = v^{x_i}$. In words, the similarity between the joint states $\boldsymbol{s}$ and $\boldsymbol{x^s}$ is the product of the similarities between the individual UV states when the elements (or states) in $\boldsymbol{x^s}$ are reordered to form the closest correspondence between the two vectors.

Thus, the weight of a sample $\boldsymbol{x} \in \Theta^{\mathcal{ST}}$ is given by

$$w^{ST}(\boldsymbol{x}|\boldsymbol{\sigma}) = f(x^\tau - \tau) \cdot \Phi(\boldsymbol{s}, \boldsymbol{x^s}), \tag{4}$$

where $f(x^\tau - \tau)$ is the same function as in Eq. 2.

The weight $w^{SS}(\boldsymbol{x}|\boldsymbol{\sigma})$ is computed similarly to $w^{ST}(\boldsymbol{x}|\boldsymbol{\sigma})$ except that only samples with an outcome x^o that matches the state of one of the UVs in the target joint state $\boldsymbol{s}$ is given nonzero probability. Thus, $w^{SS}(\boldsymbol{x}|\boldsymbol{\sigma})$ is given by:

$$w^{\mathcal{SS}}(\boldsymbol{x}|\boldsymbol{\sigma}) = \begin{cases} \Phi(\boldsymbol{s}, \boldsymbol{x^s}) \cdot f(x^\tau - \tau) & \text{if } \exists s^i \in \{\boldsymbol{s}\} : s^i = x^o \\ 0 & \text{otherwise} \end{cases} \tag{5}$$

where $\{\boldsymbol{s}\}$ denotes the set of individual UV states contained in $\boldsymbol{s}$.

III.B. Combining the Behavioral Models

The sample sets $\Theta^{\mathcal{II}}$, $\Theta^{\mathcal{NI}}$, $\Theta^{\mathcal{ST}}$, and $\Theta^{\mathcal{SS}}$, and the probability distributions over these samples sets are used by a discrete event simulation to model the human-UV system. In this discrete event simulation, detailed in Figure 1, the behavior of each UV k is defined by a sequence of states χ_k selected from the outcomes of $\Theta^{\mathcal{II}}$ (when receiving attention from the simulated operator) and $\Theta^{\mathcal{NI}}$ (when neglected by the simulated operator). The variable c_k denotes the current position of UV k in the sequence χ_k.

1. Define:
   - χ_k is state transition sequence of UV k
   - χ_k^i is the i^{th} state of the sequence χ_k.
   - $\chi_k^{c_k}$ is UV k's current state
2. Initialize:
   - Select χ_k for all k
   - Set: $c_k = 0$, $\tau = 0$, $\boldsymbol{s} = (\chi_1^{c_1}, \cdots, \chi_N^{c_N})$
3. Repeat
   a) Select switching time t from $\Theta^{\mathcal{ST}}$ w/ probabilities defined by Eqs. 1 and 4
   b) Update: $\tau = \tau + t$, $\forall k$ $c_k = c_k + t$, $\boldsymbol{s} = (\chi_1^{c_1}, \cdots, \chi_N^{c_N})$
   c) Select UV r using, $\Theta^{\mathcal{SS}}$ and Eqs. 1 and 5
   d) Select new state sequence χ_r from $\Theta^{\mathcal{II}}$ w/ probabilities defined by Eqs. 1 and 2; set $c_r = 0$
   e) Update: $\tau = \tau + |\chi_r|$, $\forall k$ $c_k = c_k + |\chi_r|$, $\boldsymbol{s} = (\chi_1^{c_1}, \cdots, \chi_N^{c_N})$
   f) Select new state sequence χ_r from $\Theta^{\mathcal{NI}}$ w/ probabilities defined by Eqs. 1 and 2; set $c_r = 0$

Figure 1. Outline of the discrete event simulation for simulating human-UV system behavior from $\Theta^{\mathcal{II}}$, $\Theta^{\mathcal{NI}}$, $\Theta^{\mathcal{ST}}$, and $\Theta^{\mathcal{SS}}$. $|\chi_r|$ denotes the length of the sequence χ_r.

In step 3a of Figure 1, operator switching time is simulated by selecting a sample from $\Theta^{\mathcal{ST}}$. During this time, the UVs in the system behave according to their current state sequences χ_k (step 3b). Once the switching time elapses, the simulated operator selects UV r to service (step 3c). A new state sequence from $\Theta^{\mathcal{II}}$ is selected to model UV r's behavior during this interaction (step 3d). When the interaction is completed, a new state sequence for UV r is selected from $\Theta^{\mathcal{NI}}$ (step 3f). The process then repeats.

In subsequent sections, we evaluate the ability of this discrete event simulation to model the performance of an observed human-UV system. Additionally, we use the discrete event simulation to predict how modifications to this observed system alter the system's performance.

III.C. Implementation Specific Modeling Parameters

While this modeling method can be used to model many human-UV systems, it requires several mission- and team-specific specifications. In particular, a set of UV states must be enumerated. As in any statistical model that uses the concept of state, the set of UV states is essential to the fidelity of the model. A good set of states must balances two objectives. First, if two situations cause, or should cause, different behaviors from either the operator or a UV in the team, they should be marked as different states. Second, a good set of UV states should be as small as possible in order to better leverage sparse data sets. As the size of the state space grows, the amount of data necessary to develop a high-fidelity model of the system will also increase substantially.

In addition to an enumeration of UV states, the model requires a state similarity metric (Eq. 3) and a time-weighting function $f(\cdot)$.

IV. Experimental Case Study

To validate the modeling method described in the previous sections, we conducted a user study of a human-UV system. In this section, we overview the software test-bed and experimental procedure used in the study, and specify the system- and mission-specific modeling parameters. In the next section, we demonstrate the descriptive and predictive abilities of models constructed from the observational data of this system.

IV.A. Software Test-bed

The user study was performed using RESCU (*R*esearch *E*nvironment for *S*upervisory *C*ontrol of *U*nmanned-Vehicles),[7] a software test-bed in which a participant directs a team of simulated UVs in a search and rescue mission. A simulated UV environment was chosen since current UV capabilities do not allow for rapid prototyping of systems that allow a single human to control multiple UVs simultaneously. Furthermore, while simulated UVs behave differently than real UVs in many respects, the modeling method described in

this paper is the same regardless of whether UVs are simulated or real.

We now overview RESCU in three parts: the team mission, the user interface, and the UVs' behaviors. Additional details about RESCU are provided in previous work.[7]

IV.A.1. Mission

Across many mission types, an operator of a human-UV system commonly assists in performing a set of abstract tasks. These abstract tasks include mission planning and re-planning, UV path planning and re-planning, UV monitoring, sensor interpretation, and target designation. RESCU captures each of these tasks in a time-critical mission.

In RESCU, an operator (the study participant) directs a team of simulated UVs to collect objects from a building over an eight-minute time period. At the end of the eight minutes, the building "blows up," destroying all UVs and objects left in it. Thus, in addition to collecting as many objects as possible, the operator must also ensure that all UVs are out of the building when time expires. Specifically, operators are asked to maximize the following objective function:

$$Score = ObjectsCollected - UVsLost, \tag{6}$$

where $ObjectsCollected$ is the number of objects collected from the building during the session and $UVsLost$ is the number of UVs remaining in the building when time expires.

An object is collected from the building using the following three-step process:

1. A UV moves to the location of an object in the building. This step requires the operator to be involved at some level in mission planning, target designation, path planning and re-planning, and UV monitoring.

2. The UV picks up the object. In real-world systems, the operator would likely need to perform particular tasks to assist the UV in this process, such as identify the object from imagery. This burden on the operator is emulated in RESCU by requiring the operator to find a U.S. city on a map.

3. The UV carries the object out of the building via one of two exits. This step requires the operator to monitor the UV and assist in path planning and re-planning.

At the beginning of a RESCU mission, the UVs are positioned outside one of two entrances of the building, and the objects are spread randomly throughout the building. The human-UV team can only see the positions of six of the objects initially. In each minute of the session, the locations of two additional objects are revealed. Additionally, the map of the building is initially unknown. The UVs create a shared map of the building as they move about it.

IV.A.2. User Interface

The user interface for these RESCU experiments was the two-screen display shown in Figure 2. The map of the building was displayed on the left screen, along with the positions of the UVs and the known objects in the building. The right screen displayed the map of the United States operators used to locate cities to assist UVs in "picking up" objects. The operator controlled a single UV at a time, which he or she selected by clicking a button on the interface corresponding to that UV. Once the operator selected the UV, he or she directed the UV by designating a goal location and modifying the UV's planned path to the goal. To designate a goal, the operator dragged the goal icon corresponding to the UV in question to the desired location. The UV then generated and displayed the path it intended to follow. The operator could modify this path with the mouse.

Two different interface modes were used. In the first mode, the operator was provided no assistance in finding U.S. cities on the map. This mode represents current UV systems in which operators must manually interpret sensor information to identify and track objects and landmarks. In the second mode, the operator was assisted by an automated visioning system (AVS), designed to model potential real-world systems that use computer vision to help identify and track objects and landmarks from imagery. The AVS suggested two cities to the operator by superimposing blinking red boxes on the map of the United States to mark the suggested cities. The suggestions made by the AVS were correct about 70-75% of the time.

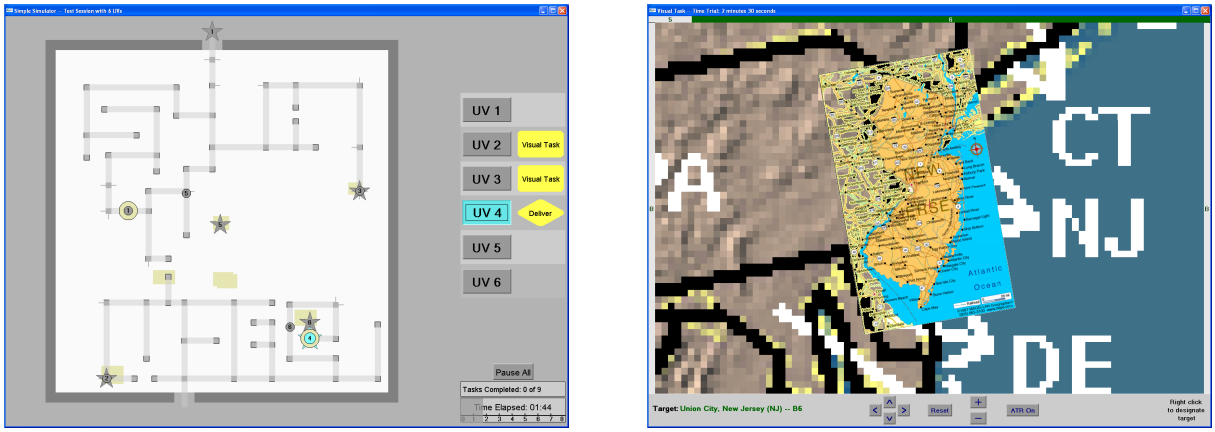

Figure 2. The RESCU user interface. The left display shows the UVs' map of the building, as well as the locations of the objects, the UVs, and their destinations. The right display shows the map of the United States for locating cities.

IV.A.3. UV Behavior

The UVs used the well-known Dijkstra's algorithm for path planning. However, since the map of the building was incomplete, the UVs had to decide, using the techniques described in pervious work,[7] between exploring the unknown portions of the building and taking a known, possibly longer, path. The resulting path planning algorithm allowed the UVs to effectively traverse the building in most situations. However, as in real-world systems, UV behavior was not always ideal. As a result, operators sometimes found it necessary to correct the UV's plans and actions.

Two different UV autonomy modes were used in the study. In the first mode, the operator manually assigned all UV goal destinations. If the operator did not provide a goal for a UV, it remained idle and did not move. This mode represents the current state-of-the-art, in which the UV used autonomous capabilities, such as "fly-by-wire" technologies, to navigate to human-designated locations. In the second mode, which represents potential UV capabilities of the future, a UV automatically selected its own goal destination in some situations. The UVs used the following rules for generating goal destinations:

1. An idle UV that was carrying an object automatically selected the nearest perceived exit for its goal destination.
2. An idle UV not carrying an object automatically selected the nearest perceived unassigned object for its goal destination.
3. In the last minute of the session, each UV automatically selected the nearest perceived exit for its goal destination.

A management-by-exception (MBE) level of automation[2] was used to allow the operator to over-rule the selections made by the UVs. The UV waited 15 seconds before executing the selection to allow the operator to override it. We refer to this mode as *MBE autonomy*.

IV.B. Experimental Procedure

The experiment was a 4 (decision support) x 4 (UV team size) mixed design study. Decision support was a between-subjects factor, where each participant was assigned a specific level. The four levels of decision support were:

1. noDS – The human-UV system was not equipped with the AVS or MBE autonomy.
2. AVS – The human-UV system was equipped with the AVS but not MBE autonomy.
3. MBE – The human-UV system was equipped with MBE autonomy but not the AVS.
4. AVS-MBE – The human-UV system was equipped with the AVS and MBE autonomy.

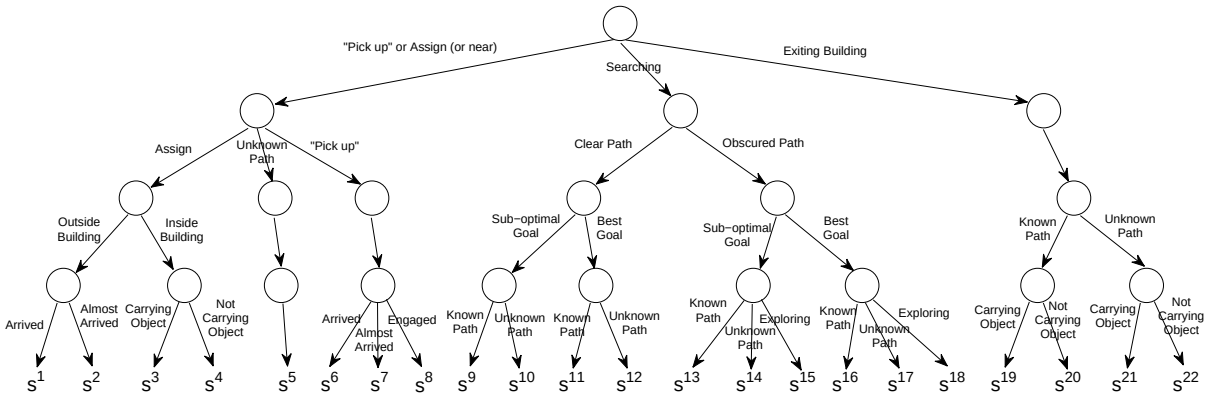

Figure 3. The decision tree used to define a UV's state in the user study.

The noDS factor level represents a system employing current UV autonomy and interface characteristics. In these systems, the mission is primarily human-guided and UVs use autonomous capabilities to navigate to human-specified locations. The other three levels represent possible future systems that leverage more advanced autonomy and intelligent interface technologies.

UV team size was a within-subjects factor, where each participant performed the search and rescue mission for team sizes of two, four, six, and eight UVs. The order of team size presented to each participant was randomized and counter-balanced throughout the study.

Each participant was randomly assigned a level of decision support and trained on all aspects of the system. The participant then completed three comprehensive practice sessions, as data showed that operator performance plateaued after three sessions. Following these practice sessions, each participant performed four test sessions, each with a different team size. After the sessions, participants answered questions about their experience in the study. Each participant was paid $10 per hour; the highest scorer also received a $100 gift certificate. Sixty-four participants between the ages of 18 and 49 participated in the study, sixteen in each level.

IV.C. Model Parameters

As outlined in Section III.C, our modeling method requires several-situation specific parameters and functions. We now define these values for RESCU, including a set of UV states, a similarity metric, and a time-weighting function $f(\cdot)$.

IV.C.1. A Set of UV States

The set of UV states should distinguish between situations that evoke, or should evoke, different behaviors from the operator or the UVs in the team. We used statistical analysis of participants' observed selection strategies as well as their post-experiment comments to identify 22 distinct UV states. Figure 3 shows a decision tree that defines these states.

Figure 3 shows that a number of features were used to determine a UV's state. These features included whether a UV was searching for an object, exiting the building, waiting for operator help to "pick up" an object, or waiting for a goal designation from the operator. A moving UV's state was further distinguished by features such as whether or not the UV was following a known path to the goal, and if another unassigned object was closer to the UV than its current goal destination.

IV.C.2. A State Similarity Metric

The similarity function $\phi(s^i, s^j)$, which defines the similarity of state s^i to state s^j (see Eq. 3), was determined from the decision tree shown in Figure 3. In the decision tree, features that had a higher impact, as determined statistically, on human and UV behavior are higher in the tree. Thus, states in the same subtree tend to have a higher similarity than those that are not in the same subtree. This point can be exploited to construct a similarity metric.

Formally, let $g(s^i, s^j)$ denote the length of the path in the decision tree from s^i to the nearest common ancestor of s^i and s^j. For example, $g(s^1, s^2) = 1$ since the states s^1 and s^2 share the same parent, whereas, $g(s^1, s^5) = 3$ since the nearest common ancestor is three levels up the tree. Then, $\phi(s^i, s^j)$ is given by

$$\phi(s^i, s^j) = \frac{1}{g(s^i, s^j)^c}, \tag{7}$$

where c is some positive integer that controls the sensitivity of the metric. Increasing c decreases the similarities between states.

IV.C.3. A Time-Weighting Function $f(\cdot)$

Recall that the time-weighting function $f(\cdot)$ is used to weight a sample based on mission time. We use a function proportional to a truncated Gaussian for $f(\cdot)$, namely

$$f(x_\tau - \tau) = \begin{cases} exp\left(-\frac{(x^\tau - \tau)^2}{2\nu^2}\right) & \text{if } (x^\tau - \tau) < W \\ 0 & \text{otherwise} \end{cases} \tag{8}$$

where ν and W are positive constants. Due to the time-critical nature of RESCU, we chose to truncate the Gaussian function (with W) so that a sample's weight was positive only if x^τ was close to τ.

V. Results

In this section, we discuss the results of the user study and use these results to evaluate our modeling method's ability to describe and predict the performance of human-UV systems. We first summarize the observed performance of the various human-UV systems observed in the user study. Next, we model the noDS human-UV systems using observational data from subjects that commanded the noDS systems in the study. Finally, we predict the performance of the AVS, MBE, and AVS-MBE systems from these models, and compare these predictions to the observed results in the study.

V.A. Observed System Performance

In the user study, system performance was determined by the number of objects collected and the number of UVs lost, depicted in Figure 4. These experimental results show several trends. First, the number of objects collected by the teams tended to increase as the size of the team increased. This trend is validated statistically. A 2x2 analysis of variance (ANOVA), with team size and decision support as the factors, shows that team size had a statistically significant impact on the number of objects collected ($F(3, 180) = 92.65$, $p < 0.001$). Tukey pairwise comparisons between systems with different team sizes show a statistically significant difference in number of objects collected between all team sizes ($p < 0.001$ in each comparison) except six- and eight-UV teams ($p = 0.663$). Thus, increasing the team size up to 6 UVs increased the number of objects the systems collected.

A second trend visible in Figure 4 is that the number of UVs lost also increased with team size ($F(3, 180) = 19.27$, $p < 0.001$). Tukey pairwise comparisons show similar trends to those seen in number of objects collected. Four-UV teams lost more UVs than two-UV teams ($p = 0.003$), six- and eight-UV teams lost more UVs than four-UV teams ($p = 0.033$ and $p = 0.001$, respectively), but there was not a statistical difference in number of UVs lost between six- and eight-UV teams. Thus, while increasing the team size caused an increase in the number of objects collected, it also increased the number of UVs that the system lost.

Figure 4 also shows that AVS support and MBE autonomy increased the number of objects the system collected, especially for larger team sizes. The ANOVA showed that the level of decision support had a statistically significant impact on number of objects collected ($F(3, 60) = 3.616$, $p = 0.018$), but not on the number of UVs lost ($F(3, 60) = 0.54$, $p = 0.655$). Tukey pairwise comparisons between the four levels of decision support show a statistical difference between the number of objects collected by the noDS and AVS-MBE systems ($p = 0.013$), but not between any of the other pairings. These results, coupled with the trends shown in the figure, suggest that the AVS and the MBE enhancements both had a positive effect on the number of objects collected by the system, though only the combined enhancements (AVS-MBE) produced a statistically significant improvement in the study. Thus, the AVS-MBE level of decision support with six or eight UVs yields the highest system performance of all the systems evaluated in the user study.

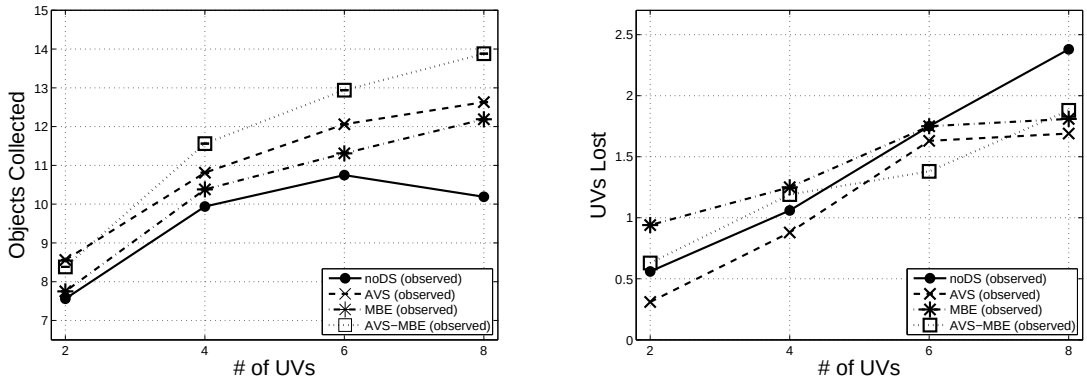

Figure 4. Mean number of objects collected (left) and UVs lost (right) observed in each experimental condition.

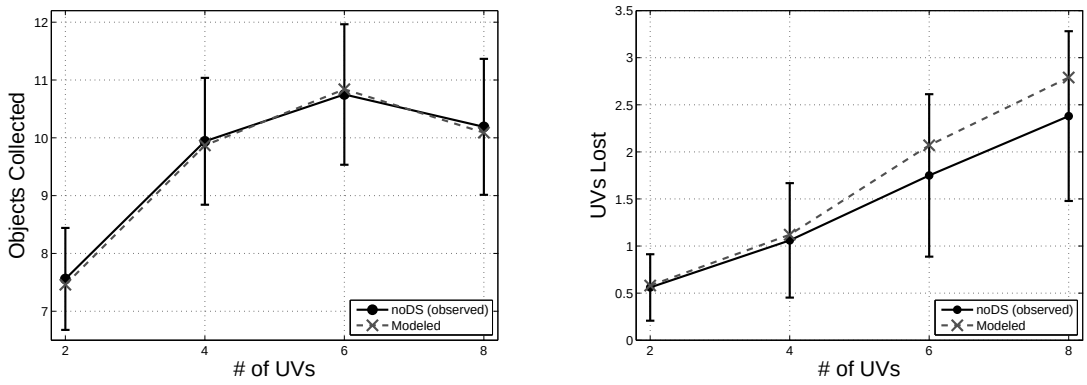

Figure 5. Comparison of observed performance of the noDS human-UV systems to model estimates of objects collected (left) and UVs lost (right). Error bars represent a 95% confidence interval on the mean.

The user study provides a rich data set for human-UV interactions in simulated future systems. Given that the noDS system represents the current state-of-the-art (primarily human-guided), this system can be modeled from observational data. This model can then predict the effects of future system enhancements, such as those present in the AVS, MBE, and AVS-MBE systems. Thus, in the remainder of this section, we analyze the ability of the modeling method described in this paper to make such predictions. We use the observational data from the noDS factor level to model the noDS system. We then use this model to predict the performance of the AVS-, MBE-, and AVS-MBE-enhanced systems without the benefit of observing them. We then compare these predictions to the results of the user study (Figure 4).

V.B. Modeling the Observed System

We constructed four separate models, one corresponding to each team size, from observational data of the noDS human-UV systems. Using the least mean squared error criteria, we set the parameters found in Eqs. 7 and 8 so that $c = 10$, $\nu = 10$ seconds, and $W = 100$ seconds. The discrete event simulation outlined in Figure 1 was then used to simulate the noDS human-UV system.

Figure 5 compares the average number of objects collected and UVs lost of the noDS system in the user study to the estimates made by the models. These estimates where found by taking the average performance of 5,000 simulations of the discrete event simulation shown in Figure 1. The models' estimates of the number of objects collected are nearly identical to observed performance. Furthermore, the models' estimates of the number of UVs lost are also reasonably good. For two- and four-UV teams, the estimates are almost identical to the observed values. However, for six- and eight-UV teams, the model slightly over-estimates the number of UVs lost, though estimates are still well within the 95% confidence intervals.

The cause for the slight inaccuracies in estimating UVs lost for larger teams appears to be tied to small inaccuracies in the models of operator selection strategies. To avoid losing UVs in RESCU, an operator

is sometimes required to make precise time-critical decisions in order to ensure that UVs exit the building before time expires, whereas the same time-critical precision is not required to collect objects. As the joint state space becomes larger with larger teams, the relatively small number of data samples compared to the size of the joint state space makes it difficult to model operator strategies with sufficient precision. As a result, the model slightly over-estimates the number of UVs lost in larger UV teams.

Despite these small inaccuracies, the estimates are, overall, reasonably good. The models effectively describe the observed system. However, these results do not demonstrate predictive ability since the model is only duplicating observed results. To be predictive, the model must be able to predict the performance of unobserved systems.

V.C. Predicting the Effects of System Design Modifications

We now evaluate the models' ability to predict the performance of the system with the AVS, MBE, and AVS-MBE enhancements.

V.C.1. Predicting the Effects of the AVS Support

To predict how the AVS enhancement would change system performance, we must determine the aspects of the team that would be affected by the AVS and how they would be changed. These changes must be reflected in the individual samples, which entails either deriving a new set of samples, or editing the existing samples. We use the latter approach in this paper.

Since the AVS affects human-UV interactions, it will mostly affect $\mathcal{II}$; we assume that the other aspects of the system are left unchanged. To capture the change in $\mathcal{II}$ induced by the AVS enhancement, we edit the outcome x^o of each sample $\boldsymbol{x} \in \Theta^{\mathcal{II}}$ in which the operator assisted a UV in "picking up" on object by locating a city on the map of the United States. In these samples, the amount of time taken to identify the city should be altered to reflect the change induced by the AVS support.

For example, consider the following outcome of a hypothetical sample of interaction impact:

$$s^6, s^6, s^6, s^8, s^8, s^8, s^8, s^8, s^8, s^8, s^8, s^8, s^8, s^8, s^3, s^3, s^3, s^{18}, s^{18}$$

From the state tree shown in Figure 3, we can deduce that state s^8 corresponds to situations in which the operator and UV are engaged in "picking up" an object. In the state transition sequence, this process takes eleven time units, beginning with the 4^{th} element of the sequence and ending with the 14^{th} element of the sequence. To estimate the effects of the AVS support, we remove this subsequence and replace it with a subsequence reflecting the amount of time the process would take with the AVS support. For example, if we have cause to believe that it would take the operator just six time units with the AVS support, then the edited sequence would be:

$$s^6, s^6, s^6, s^8, s^8, s^8, s^8, s^8, s^8, s^3, s^3, s^3, s^{18}, s^{18}.$$

Note, however, that since the effects of the AVS support are not completely known *a priori*, we must estimate what they might be, or evaluate the proposed automated visioning system. We estimated the length of time it takes operators to locate a city in a separate evaluation of the AVS support, and substituted these times into the appropriate samples in $\Theta^{\mathcal{II}}$. On average, we observed that the AVS support reduced the time it took operators to locate the city by approximately five seconds.

After editing the samples in this way, we simulated the AVS-enhanced system using the discrete event simulation outlined in Figure 1. We then adjusted the simulation's predictions of system performance to account for the initial errors present in the model. Specifically, we multiplied the simulation's predictions by the ratio of the observed values to the model estimates in Figure 5. The resulting predictions are compared to the observed performance in the user study in Figure 6. For each team size, the predictions are reasonably accurate for both number of objects collected and UVs lost, as all predictions fall within the 95% confidence intervals. Thus, the models effectively predicted the affects of the AVS enhancement.

V.C.2. Predicting the Effects of the MBE Autonomy

The MBE autonomy alters a UV's behavior in the absence of interactions. Thus, whereas the AVS support primarily affected $\mathcal{II}$, the MBE autonomy primarily affects $\mathcal{NI}$. As such, to simulate the effects of the MBE autonomy, we must modify the samples in $\Theta^{\mathcal{NI}}$ to reflect this new behavior.

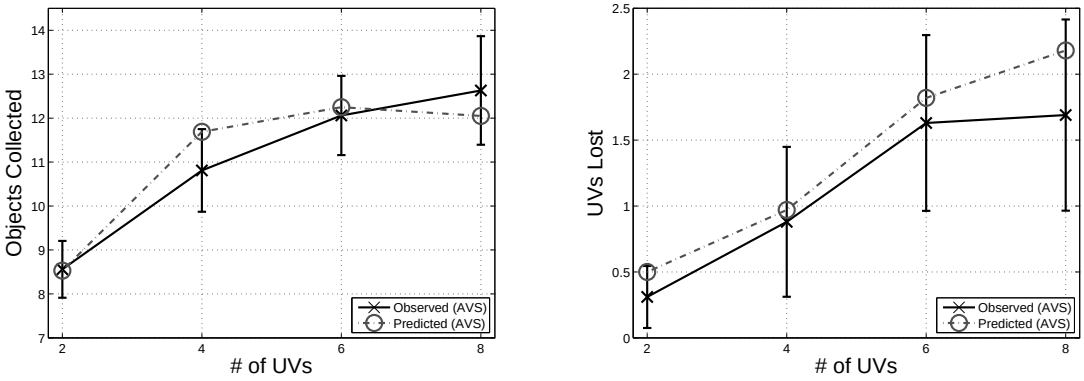

Figure 6. Comparison of model predictions to observed data from the AVS system. Error bars represent a 95% confidence interval on the mean.

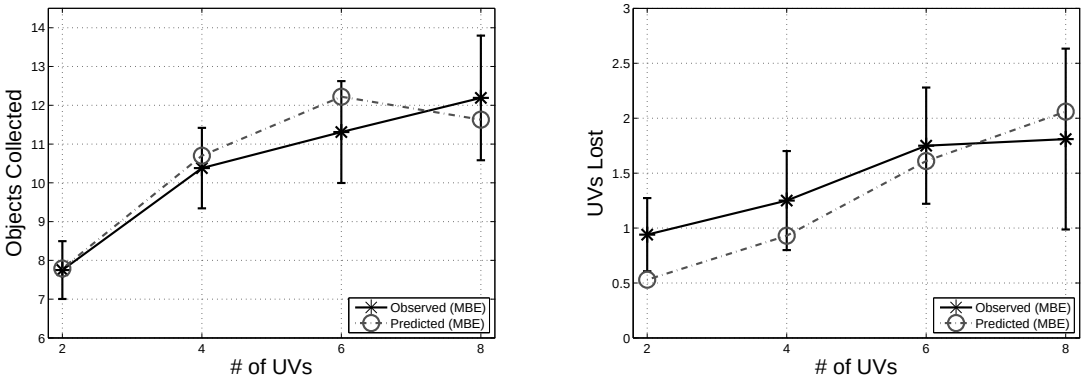

Figure 7. Comparison of model predictions to observed data from the MBE system. Error bars represent a 95% confidence interval on the mean.

To estimate how each sample $\boldsymbol{x} \in \Theta^{\mathcal{NI}}$ would change due to the MBE enhancement, we must first identify when MBE autonomy would cause changes in each sample's outcome, or state transition sequence. This is easily done using the three rules outlined in Section IV.A.3. For example, consider the following state transition sequence:

$$s^{19}, s^{19}, s^{19}, s^2, s^2, s^2, s^1, s^1, s^1, s^1, s^1, s^1, s^1, s^1, s^1, s^1, s^1, s^1, s^1, s^1, s^1, s^1, s^1, s^1, \cdots$$

Using the decision tree shown in Figure 3, we can deduce that this sequence corresponds to the situation in which a UV finishes carrying an object out of the building and then waits (in state s^1) to be given a new goal destination. Given the second rule of MBE autonomy, which specifies that the UV will automatically set a new goal for itself after waiting in state s^1 for 15 seconds, we can infer that the MBE autonomy would cause the UV to leave state s^1 and re-enter the building after 15 time units (assuming a time unit equals one second).

Second, we must determine how to change sequences that would be altered by the MBE autonomy. This is achieved by identifying sequences from $\Theta^{\mathcal{NI}}$ that corresponded to times in which the operator had, in the previous interaction, assigned a UV in state s^1 a new goal destination. These existing sequences can then replace the portions of the sequences we wish to edit. Thus, continuing our example, the state transition sequence could become:

$$s^{19}, s^{19}, s^{19}, s^2, s^2, s^2, s^1, s^1, s^1, s^1, s^1, s^1, s^1, s^1, s^1, s^1, s^1, s^1, s^1, s^1, s^1, s^{11}, s^{11}, s^{11}, \cdots$$

which shows the UV re-entering the building in search of another object after waiting for 15 time units.

After modifying the samples in $\Theta^{\mathcal{NI}}$ as described, we predicted the performance of the MBE-enhanced system using the discrete event simulation (average of 5,000 simulations). Figure 7 compares these predictions to the performance of the MBE-enhanced system we observed in the user study. With respect to the number

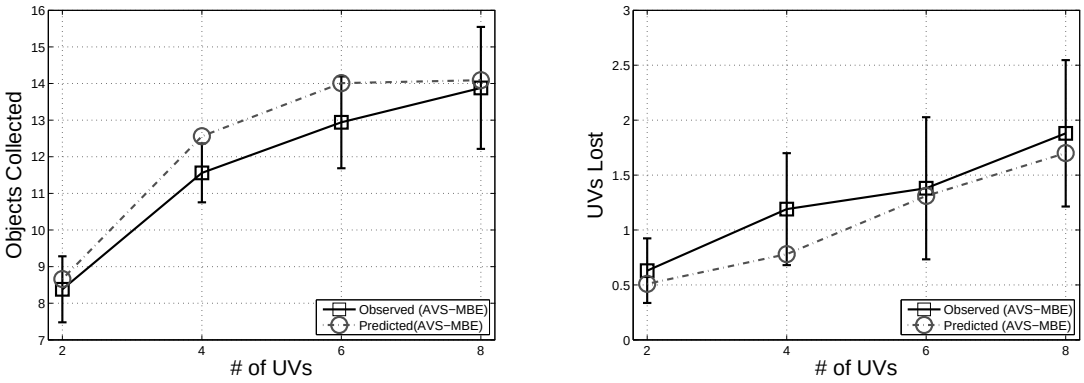

Figure 8. Comparison of model predictions to observed data from the AVS-MBE system. Error bars represent a 95% confidence interval on the mean.

of objects the system collected, the figure shows that the model makes reasonably good predictions for each team size, as all predictions fall within the 95% confidence interval. However, the predictions for UVs lost, though accurate for six- and eight-UV teams, are low for smaller UV teams. This is particularly true of the two-UV case, in which the prediction is outside the 95% confidence interval. While the model predicted that the MBE autonomy would reduce the number of UVs lost for smaller teams, they were actually higher in the user study. While this trend is not statistically significant, one possible, yet unsubstantiated, explanation for this unexpected result is that operator's over-trusted the MBE autonomy. Since the model does not explicitly account for operator trust, it would be unable to predict this effect. We leave further analysis of this point to future work.

V.C.3. Predicting the Effects of the AVS-MBE Enhancement

The AVS-MBE enhanced system can be simulated by combining the changes in the models used to simulate the AVS- and MBE-enhancements individually. Figure 8 compares predictions of system performance made by the models against those observed in the user study. Once again, the predictions made by the model are reasonable, though not perfect. For each team size, the predictions of objects collected are higher than the observed results, while the predictions of UVs lost are lower than the observed results. However, with the exception of objects collected in the four-UV condition, all predictions are with the 95% confidence interval. Thus, the models were reasonably effective in predicting the effects of multiple design changes.

V.D. Implications for Human-UV System Design

The results in this section demonstrate that the modeling method presented in this paper can be used to both describe and predict the performance of human-UV systems under certain assumptions (more on this in Section VI). Thus, it can be useful to designers of human-UV systems. For example, consider the situation in which the noDS system has been designed, implemented, and deployed. Since this system often loses a substantial number of UVs and collects, on average, no more than half of the total possible objects (Figure 4), it is desirable to know how to alter the system to improve its performance.

The predicted effects of the AVS, MBE, and AVS-MBE enhancements for various metrics of system performance are shown together in Figure 9. The predictions identify several key insights into the AVS, MBE, and AVS-MBE enhancements. First, the predictions indicate that each of the design enhancements would increase the effectiveness of the system. Implemented alone, the models predict that the AVS and MBE enhancements would produce moderate improvements for each team size as shown in Table 6. While the MBE and AVS enhancements are predicted to have similar impact on the system's performance in larger teams, the AVS enhancement would be more effective for two- and four-UV teams. This predicted trend is verified by the outcomes of the user study (Figure 4).

However, these predicted increases in system score are potentially misleading, as system designers must also consider the costs of performance increases. Since increases in UV capabilities would likely increase the

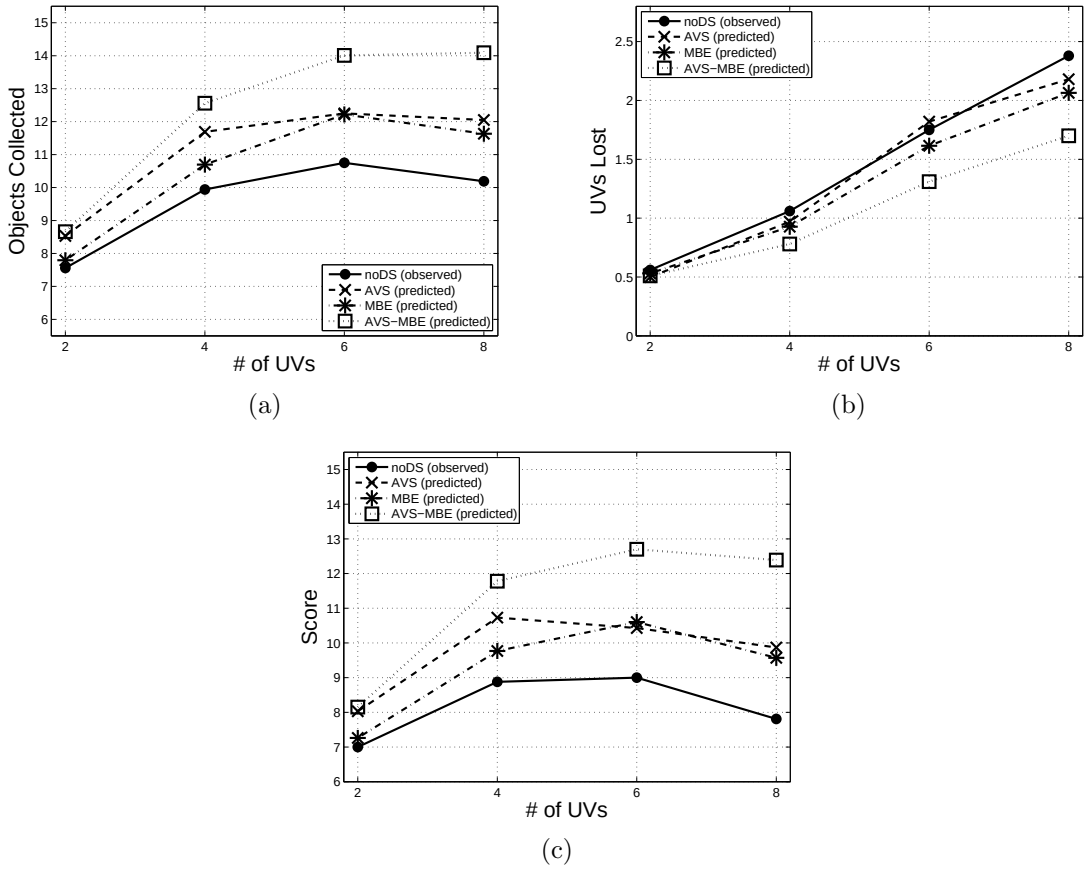

Figure 9. Comparison of the predicted performance of various design improvements with respect to (a) objects collected, (b) UVs lost, and (c) system score.

UVs' cost, a system designer must also alter the system objective function from Eq. 6 to:

$$Score = ObjectsCollected - (UVCostRatio \cdot UVsLost), \tag{9}$$

where $UVCostRatio$ is the ratio of the cost of a UV equipped with AVS and MBE capabilities to the cost of a UV in the original implementation (noDS).

Figure 10 shows the effects that different values of $UVCostRatio$ have on the predicted system scores of the AVS-MBE-enhanced system. Even when the cost of a UV is doubled, the model predicts that the AVS-MBE-enhancement would still increase the system score substantially for each team size (Table 6).

VI. Conclusions and Future Work

In this paper, we have described a method for modeling human-UV systems consisting of a single operator and multiple UVs. In this model, the stochastic behavior of both the operator and the UVs are constructed from observational data. Together, these stochastic models describe the complete human-UV system. Furthermore, via user study, we demonstrated that they can be used to predict the affects of alterations in the human-UV systems, such as changes to the human-UV interface or UV autonomy levels. These results demonstrate that this modeling method can have significant implications for the design and implementation of future human-UV systems.

While these results are encouraging, the modeling method has a number of limitations that limit its generality, each of which should be addressed in future work. First, when predicting the effects of design changes, the model assumes that alterations in the system will have limited impact on other aspects of the human-UV system. For example, in Section V, we assumed that the AVS support would only affect interaction impact and that the MBE autonomy would only alter neglect impact. While verifying the correctness of these assumptions is difficult in our study due to the limited amount of observational data in

Table 6. Predicted percentage of performance increase in system score (Eq. 6) for the various system enhancements.

System	2 UVs	4 UVs	6 UVs	8 UVs
AVS	15%	21%	16%	26%
MBE	4%	10%	18%	23%
AVS-MBE	16%	33%	41%	59%
AVS-MBE (2x UV cost)	9%	24%	27%	36%

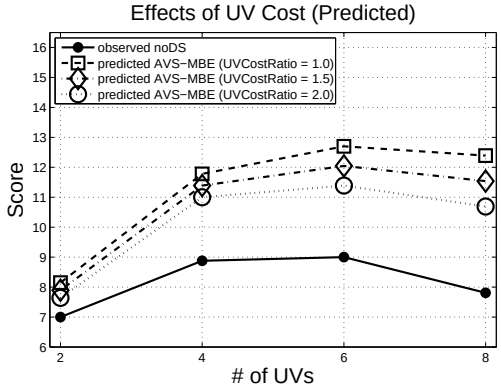

Figure 10. Predicted system score of the AVS-MBE enhanced system for various $UVCostRatio$'s.

conjunction with a large state space, the accuracy of the models' predictions indicate that these assumptions are reasonably good. However, it is reasonable to assume that these assumptions would fail for other design modifications, particularly those that give rise to cognitive phenomena related to operator workload,[19] operator utilization,[20–22] operator trust in automation,[23,26] and operator situation awareness.[24,25]

Second, the model we presented in this paper assumes that the human-UV team consists of a single operator and multiple UVs performing independent tasks. However, many systems require that UVs cooperate,[27] which introduces a level of dependence not accounted for in this model. Third, in this paper, we assumed that the operator interacted with a single UV at a time. The model could potentially be extended to allow the operator to interact with groups of UVs.[6,28]

Despite these limitations, the modeling method presented in this paper shows significant promise for modeling complex human-UV systems for both descriptive and predictive purposes.

Acknowledgments

This work was funded by MIT Lincoln Laboratory.

References

[1]A. P. Tvaryanas, W. Platte, C. Swigart, J. Colebank, and N. L. Miller. A resurvey of shift work-related fatigue in MQ-1 Predator unmanned aircraft system crewmembers. Technical Report NPS-OR-08-001, Naval Postgraduate School, Monterey, CA, March 2008.

[2]T. B. Sheridan and W. L. Verplank. Human and computer control of undersea teleoperators. Technical report, Man-Machine Laboratory, Massachusetts Institute of Technology, Cambridge, MA, 1978.

[3]P. J. Mitchell, M. L. Cummings, and T. B. Sheridan. Mitigation of human supervisory control wait times through automation strategies. Technical report, Humans and Automation Laboratory, Massachusetts Institute of Technology, June 2003.

[4]D. B. Kaber and M. R. Endsley. The effects of level of automation and adaptive automation on human performance, situation awareness and workload in a dynamic control task. *Theoretical Issues in Ergonomics Science*, 5(2):113–153, 2004.

[5]J. Wang and M. Lewis. Human control for cooperating robot teams. In *Proceeding of the 2nd Annual Conference on Human-robot Interaction*, pages 9–16, 2007.

[6]M. A. Goodrich, T. W. McLain, J. D. Anderson, J. Sun, and J. W. Crandall. Managing autonomy in robot teams: observations from four experiments. In *Proceeding of the 2nd Annual Conference on Human-robot Interaction*, pages 25–32, 2007.

[7]J. W. Crandall and M. L. Cummings. Identifying predictive metrics for supervisory control of multiple robots. *IEEE Transactions on Robotics*, 23(5), October 2007.

[8]M. A. Goodrich, D. R. Olsen Jr, J. W. Crandall, and T. J. Palmer. Experiments in adjustable autonomy. In *Proceedings of IJCAI Workshop on Autonomy, Delegation and Control: Interacting with Intelligent Agents*, 2001.

[9]D. R. Olsen Jr. and S. B. Wood. Fan-out: Measuring human control of multiple robots. In *Proceedings of the Conference on Human Factors in Computing Systems*, 2004.

[10]J. W. Crandall, M. A. Goodrich, D. R. Olsen Jr., and C. W. Nielsen. Validating human-robot systems in multi-tasking environments. *IEEE Transactions on Systems, Man, and Cybernetics – Part A: Systems and Humans*, 35(4):438–449, 2005.

[11]D. R. Olsen Jr. and M. A. Goodrich. Metrics for evaluating human-robot interactions. In *NIST's Performance Metrics for Intelligent Systems Workshop*, Gaithersburg, MA, 2003.

[12]T. B. Sheridan and M. K. Tulga. A model for dynamic allocation of human attention among multiple tasks. In *Proceedings of the* 14^{th} *Annual Conference on Manual Control*, 1978.

[13]S. Mau and J. Dolan. Scheduling to minimize downtime in human-multirobot supervisory control. In *Workshop on Planning and Scheduling for Space*, 2006.

[14]H. Neth, S. S. Khemlani, B. Oppermann, and W. D. Gray. Juggling multiple tasks: A rational analysis of multitasking in a synthetic task environment. In *Proceedings of the* 50^{th} *Annual Meeting of the Human Factors and Ergonomics Society*, 2006.

[15]P. Squire, G. Trafton, and R. Parasuraman. Human control of multiple unmanned vehicles: effects of interface type on execution and task switching times. In *Proceeding of the* 1^{st} *Annual Conference on Human-robot Interaction*, pages 26–32, New York, NY, USA, 2006. ACM Press.

[16]M. A. Goodrich, M. Quigley, and K. Cosenzo. Task switching and multi-robot teams. In *Proceedings of the Third International Multi-Robot Systems Workshop*, 2005.

[17]M. L. Cummings and P. J. Mitchell. Predicting controller capacity in remote supervision of multiple unmanned vehicles. *IEEE Transactions on Systems, Man, and Cybernetics – Part A Systems and Humans*, 38(2):451–460, 2008.

[18]M. L. Cummings, C. Nehme, J. W. Crandall, and P. J. Mitchell. Predicting operator capacity for supervisory control of multiple UAVs. *Innovations in Intelligent UAVs: Theory and Applications,* Ed. L. Jain, 2007.

[19]R. M. Yerkes and J. D. Dodson. The relation of strength of stimulus to rapidity of habit-formation. *Journal of Comparative Neurology and Psychology*, 18:459–482, 1908.

[20]D. K. Schmidt. A queuing analysis of the air traffic controller's workload. *IEEE Transactions on Systems, Man, and Cybernetics*, 8(6):492–498, 1978.

[21]W. B. Rouse. *Systems Engineering Models of Human-Machine Interaction.* New York: North Holland, 1983.

[22]M. L. Cummings and S. Guerlain. Developing operator capacity estimates for supervisory control of autonomous vehicles. *Human Factors*, 49(1):1–15, 2007.

[23]J. D. Lee and N. Moray. Trust, self-confidence, and operators' adaptation to automation. *International Journal of Human-Computer Studies*, 40(1):153–184, January 1994.

[24]M. R. Endsley. Design and evaluation for situation awareness enhancement. *Proceedings of the Human Factors Society 32nd Annual Meeting*, pages 97–101, 1988.

[25]J. Drury, J. Scholtz, and H. A. Yanco. Awareness in human-robot interactions. In *Proceedings of the IEEE Conference on Systems, Man and Cybernetics*, Washington, DC, 2003.

[26]M. L. Cummings. Automation bias in intelligent time critical decision support systems. In *AIAA* 1^{st} *Intelligent Systems Technical Conference*, pages 33–40, September 2004.

[27]J. Wang and M. Lewis. Assessing cooperation in human control of heterogeneous robots. In *Proceeding of the 3rd Annual Conference on Human-robot Interaction*, pages 9–16, 2008.

[28]C. Miller, H. Funk, P. Wu, R. Goldman, J. Meisner, and M. Chapman. The playbook approach to adaptive automation. In *Proceedings of the Human Factors and Ergonomics Society 49th Annual Meeting*, 2005.